Kobe University Repository : Kernel

PDF issue: 2025-12-05

Effects of air temperature, humidity, and wind velocity distribution on indoor cooling load and outdoor human thermal environment at urban scale

Takebayashi, Hideki

(Citation)
Energy and Buildings,257:111792

(Issue Date)
2022-02-15

(Resource Type)
journal article

(Version)
Accepted Manuscript

(Rights)
© 2021 Elsevier B.V.
This manuscript version is made available under the Creative Commons Attribution-NonCommercial-NoDerivatives 4.0 International license.

(URL)
https://hdl.handle.net/20.500.14094/90009038

KOBE UNIVERSITY

Tittle:

Effects of air temperature, humidity, and wind velocity distribution on indoor cooling load and outdoor human thermal environment at urban scale

Abstract:

In recent years, adaptations to extreme urban high temperatures such as awnings, louvers, directional reflectors, misters, and evaporative materials have been expected to address the outdoor human thermal environment under the influence of urban heat islands. In order to implement these countermeasure technologies in appropriate locations in urban areas, it is necessary to identify the locations where the countermeasure technologies are needed. It is also important to understand the distribution of thermal environmental indicators at the urban scale so that the results can be reflected in urban planning. In this study, I analyzed the distribution of thermal environmental indices during the summer days using mesoscale weather research and forecasting model. I analyzed the distribution of thermal environmental indices in the coastal cities of Tokyo, Osaka, and Nagoya, where there is concern about the increase in indoor cooling load and the risk of heat stoke due to the increase in humidity caused by the inflow of sea breezes, and examined the possible adverse effects of increased humidity. In the three areas, although humidity was high near the coast, the thermal environment indices, wet bulb globe temperature, standard new effective temperature, and physiological equivalent temperature, were low due to low air temperatures and high

wind velocities. The enthalpy increased slightly, but the effect on the indoor cooling load was small. It also compares the distribution of thermal environment indices and the effects of the introduction of adaptation measures. Solar shading is more effective than moving to near the coast, urban ventilation and mist spray.

Key words: adaptation measures, coastal cities, thermal environment indices, indoor cooling load, adaptive city

Nomenclature

MRT: Mean Radiant Temperature [°C]

NVI: Normalized Vegetation Index

PET: Physiological Equivalent Temperature [°C]

SET*: Standard New Effective Temperature [°C]

WBGT: Wet Bulb Globe Temperature [°C]

WRF model: Weather Research and Forecasting model

Q: ventilation cooling load [W]

V: ventilation rate [m^3/s]

ρ: air density [g/m^3]

Ho: outdoor specific enthalpy [J/g]

Hi: indoor specific enthalpy [J/g]

Cp: specific heat of air [J/(gK)]

l: latent heat of evaporation [J/g]

ΔTo: air temperature increase [K]

ΔXo: humidity increase [g/g]

u2: wind velocity at 2 m high [m/s]

u10: wind velocity at 10 m high [m/s]

Metabolic rate [met]: (1 met = 58.2 W/m^2)

Clothes [clo]: (1 clo = 0.155 Km^2/W)

1. Introduction

Mitigation measures such as rooftop greening, cool roofs (highly reflective materials), and water retention materials were developed with the expectation that they would counter urban heat islands. Akbari and Kolokotsa [1] reviewed the development and evaluation of materials to counter the effects of summertime urban heat islands, including cool roofs, cool pavements, and urban vegetation. Aleksandrowicz et al [2] analyzed the research trends in urban heat island mitigation through a comprehensive survey. They assessed the areas of research interest in mitigation measures. Santamouris [3] summarized the mitigation potential of reflective roofs and green roofs through a review of related papers including detailed analytical conditions. Santamouris [4] described the current state of the art in the field of reflective, permeable and water retaining pavements to counter the heat island effect of pavements, which occupy a very high percentage of urban areas. In recent years, adaptive measures such as sunshades, louvers, directional reflectors, mists, and evaporative materials have been developed to address the thermal environment of humans outdoors affected by urban heat islands [5].

In order to implement these countermeasure technologies in appropriate locations in urban areas, it is necessary to identify the locations where the countermeasure technologies are needed. Since adaptation is about improving the thermal environment of the human body locally [6], it is important to extract hot spots where radiation and wind predominate at the district scale [7]. In addition, it is important to understand the distribution of thermal environment indicators at the city scale in order to reflect them in

urban planning. Ohashi et al [8] analyzed the distribution of WBGT (Wet Bulb Globe Temperature) in the 23 wards of Tokyo. It is noted that WBGT is higher in inland wards, but the risk of heat stroke is higher in urban wards because the daytime population is considered. It has also been calculated that higher reflectance of roads, walls and roofs increases WBGT and the risk of heat stroke [9]. Therefore, they concluded that heat island mitigation measures that reflect solar radiation may significantly increase the hazard and risk of outdoor heat stress in urban areas. In addition, Kasai et al [10] predicted the future risk of heat stroke using WBGT as an indicator in the Tokyo area. The results showed that the risk in coastal areas will increase by more than 20% in the 2030s due to changes in climatic conditions such as increased humidity.

Many studies have been carried out at the district scale. Eliasson [11] pointed out that some of the changes in surface temperature in urban canyons could be explained by sky view factors. Outdoor thermal comfort in urban street canyons of various shapes and orientations has been studied by Ali-Toudert et al [12, 13], who found that shading is an important strategy to alleviate outdoor heat stress in hot summer conditions. The percentage and location of shadow areas in open spaces, which depend on the position of the sun and the urban form, has been analyzed by Martinelli et al [14]. Tree shading has a significant effect on human thermal comfort, as expressed by physiological equivalent temperature, and has been studied by Abreu-Harbich et al [15]. As shown by Algeciras et al [16], the spatial distribution of thermal conditions at the street level is strongly dependent on the aspect ratio and the orientation of the street. The effect of trees on

92 human thermal comfort has been quantified by Lee et al [17] on a heat wave day. The
93 impact of different vegetation species on the outdoor thermal environment has been
94 evaluated by S. Zheng et al [18] using numerical simulations.
95 Research at the urban scale is also important for examining strategies for introducing
96 adaptation measures appropriate to the region. The authors used the Mesoscale Weather
97 Research and Forecasting (WRF) model to analyze the characteristics of daytime air
98 temperature distributions during good summer weather in five coastal cities in Japan and
99 an inland city in Germany of different sizes [19]. In Japan's coastal cities, air temperatures
100 were found to increase with increasing distance from the coast. Since high temperatures
101 in summer affect both the deterioration of the human thermal environment outdoors and
102 the increase in indoor cooling load and cooling energy, it is necessary to understand the
103 actual situation in order to consider more appropriate countermeasures. This study
104 analyzes the effects of air temperature, humidity, and wind velocity distributions at the
105 urban scale on indoor cooling loads and outdoor human thermal environments. These
106 distributions are then compared to the effects of introducing adaptation measures. The
107 purpose of this study is to examine various strategies for introducing adaptation measures
108 based on a comparison with the spatial distribution of thermal environmental indices at a
109 scale covering the entire metropolitan area.
110 The flow of this study is as followed. Initially, the WRF model is used to calculate air
111 temperature, humidity, and wind velocity distributions over a 100 km square area with a 1
112 km grid. The increase in cooling load due to room ventilation is then calculated using the

113 spatial distribution of air temperature and humidity and the recommended ventilation
114 volume. In addition, outdoor thermal environment indices are calculated using the
115 distributions of air temperature, humidity, and wind velocity. Based on the comparison
116 with the spatial distribution obtained above, various strategies for introducing adaptation
117 measures will be discussed.
118
119 2. Methods
120 2.1 Mesoscale calculation
121 The Mesoscale Weather Research and Forecasting Model (WRF) (version 3.0.1.1-ARW)
122 was used for the calculations. The WRF model is a next-generation mesoscale numerical
123 weather prediction system for both atmospheric research and operational forecasting.
124 The model has a wide range of meteorological applications on scales from tens of meters
125 to thousands of kilometers [20]. The Mellor–Yamada–Janjic model was used for the
126 turbulent closure model (planetary boundary layer scheme). The Noah-LSM was applied to
127 the land surface model and the urban canopy model was applied to the urban area
128 (Kusaka et al [21]). Figure 1 shows the objective study areas. Domain 1, which is 360 km
129 square with a 3 km grid, is the outer area, and Domain 2, which is 103 km square with a 1
130 km grid, is the inner area. A two-way nesting approach was applied between the two
131 regions. The latitude and longitude of each objective city are as follows; Tokyo: N35.5°,
132 E139.3°, Osaka: N34.4°, E135.1°, Nagoya: N35.0°, E136.5°. For the analysis, the calculated

results of air temperature and relative humidity at a height of 2 m and wind velocity at a height of 10 m in Domain 2 were used.

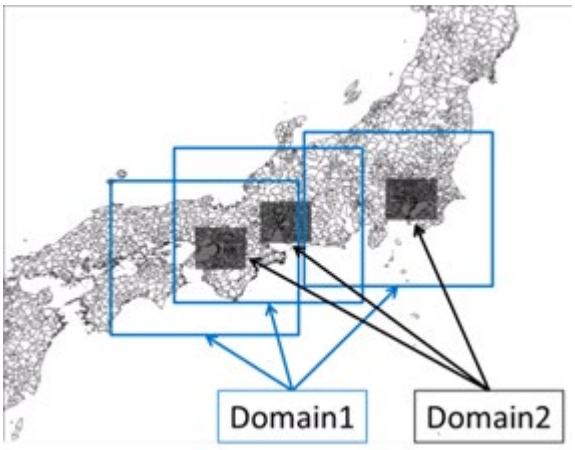

Figure 1 Objective study areas in Tokyo, Osaka and Nagoya (Domain 1: 3 km grid, 360 km square, Domain 2: 1 km grid, 103 km square).

The calculation conditions are shown in Table 1. The period for calculation is from August 1 to 31, 2010. In order to use the urban canopy model (Kusaka et al. [21]), based on digital national land information (spatial resolution of 100 m) and the normalized vegetation index (NVI) created from and Landsat7 ETM+ data averaged within a 1 km square grid of WRF, urban areas were classified into three categories according to a previous study (Kitao et al. [22]); Urban A: high-rise and high-density (mean building height: 10 m, gross building ratio: 44 %), Urban B: middle-rise and moderate-density (mean building height: 7.5 m, gross building ratio: 38 %), Urban C: low-rise and low-density (mean building height: 5 m, gross building ratio: 29 %).

Table 1 Calculation conditions for WRF model.

Calculation period	August 1 - 31, 2010
Vertical mesh	28 layers from ground surface to 100 hPa
Horizontal mesh	Domain 1: 3 km (120 * 120 grids),
	Domain 2: 1 km (103 * 103 grids)
Meteorological data	JMA: Meso-scale analysis (3 hourly, 10 km grids, 20 layers),
	NCEP: Final analysis (6 hourly, 1 degree grids, 17 layers)
Geographical data	Terrain height: Digital map (50 m resolution),
	Land use: Digital national land information (about 100 m resolution) + NVI (Landsat ETM+, November 5, 2001)
Microphysics process	Purdue Lin et al. scheme
Radiation process	Long wave: RRTM longwave scheme
	Short wave: Dudhia shortwave scheme
Planetary boundary layer process	Mellor-Yamada-Janjic PBL scheme
Surface process	Urban area: Urban canopy model,
	Non-urban area: Noah LSM
Cumulus parameterization	None
Four-dimensional data assimilation	None

Figure 2 shows the land use conditions and the number of urban meshes in Tokyo, Osaka, and Nagoya. The number of urban land uses (Urban A, B, and C) in a 1 km square mesh is 3,698 in Tokyo, 1,271 in Osaka, and 1,416 in Nagoya. Figure 3 shows the frequency of urban land use (Urban A, B, and C) on a 1 km square mesh at each distance point from the coast. The distance from the coast is the distance between each point and the nearest coast. The frequency of urban land use on a 1 km square mesh is greater in coastal areas and gradually decreases in inland areas. In Tokyo, the number of urban land uses on a 1km square mesh is much larger than in other cities from the coast to the inland. The number

of urban land uses in a 1km square mesh in the coastal area of Nagoya is slightly smaller than in Tokyo and Osaka.

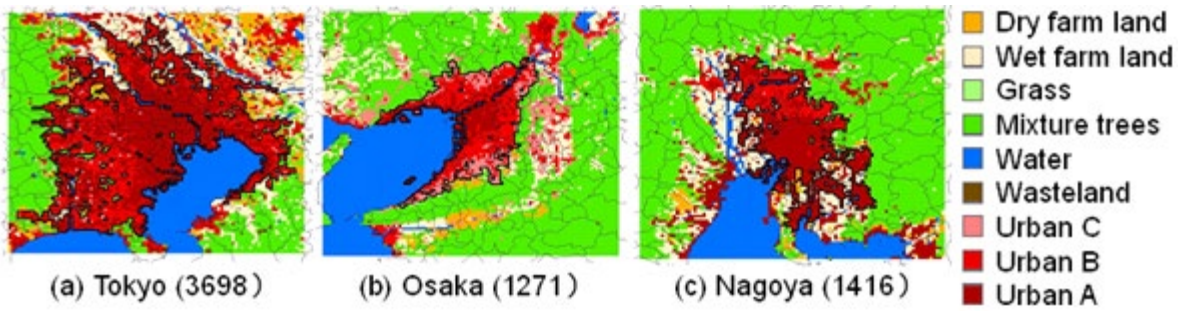

Figure 2 Land use conditions and the number of urban land uses (Urban A, B, and C) in a 1 km square mesh in (a)Tokyo, (b)Osaka, and (c)Nagoya (1 km grid, 103 km square). Areas of continuous urban land use are indicated by black frames.

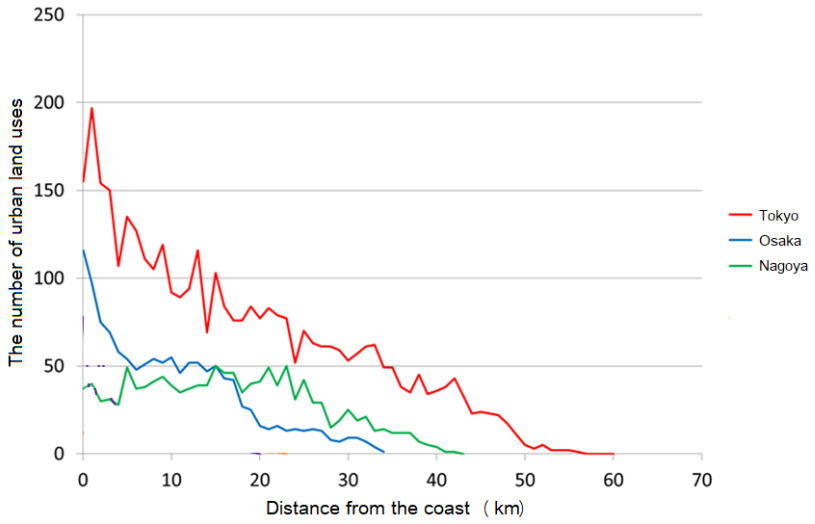

Figure 3 Frequency of urban land use (Urban A, B, and C) on a 1 km square mesh at each distance point from the coast.

The conditions for fine days were selected according to the following meteorological conditions; weather: mostly sunny and sunny, sunshine hours: 7.0 hours or more, solar radiation: 19 MJ/m^2 or more, and precipitation: 0.5 mm or less. The conditions of the sea breeze were as follows according to the meteorological conditions; wind velocity: more than 2.0 m/s at observatory, wind direction: the main wind direction at each observatory, and duration: more than 6 hours under the above conditions.

2.2 Indoor cooling load

The increase in air temperature and humidity leads to an increase in cooling load due to the intake of fresh outside air for indoor ventilation.

The ventilation cooling load Q is calculated by the following equation (1).

$$Q = V \rho (Ho - Hi) \quad (1)$$

The increase in ventilation cooling load ΔQ is calculated by the following equation (2).

$$\Delta Q = V \rho \Delta Ho = V \rho (Cp \Delta To - l \Delta Xo) \quad (2)$$

Currently in Japan, the ventilation rate V is recommended to be 30 m^3/h per person for infection control. At the same time, a social distance of, for example, 2 m is recommended, so no increase in the ventilation rate V is assumed for infection control. Therefore, the increase in ventilation cooling load ΔQ can be considered to be solely due to the increase in outdoor air enthalpy ΔHo (air temperature ΔTo and humidity ΔXo). Since the ventilation volume V given here is close to the value conventionally used in Japan, the cooling load due to ventilation calculated with this value is also a typical value.

When assuming a room with a high occupancy density, it is necessary to assume a larger ventilation volume.

2.3 Outdoor human thermal environment

WBGT (Wet Bulb Globe Temperature) is calculated from dry bulb temperature, wet bulb temperature, and black bulb temperature. Wet bulb temperature is calculated from air temperature and humidity. Although black bulb temperature varies locally due to the influence of urban morphology, it is assumed to be a constant value (40 °C) because this is a mesoscale analysis. SET* (Standard New Effective Temperature) and PET (Physiological Equivalent Temperature) are calculated from air temperature, humidity, wind velocity, mean radiative temperature, metabolic rate, and clothes. Although wind velocity and mean radiative temperature vary locally due to the urban morphology, wind velocity at a height of 2 m (u2) is calculated from wind velocity at a height of 10 m (u10) using a constant wind velocity ratio (u2/u10 = 0.2), and mean radiative temperature is assumed to be a constant value (40 °C) because this is a mesoscale analysis. Metabolic rate and clothes are set to 1.4 Met and 0.6 clo, assuming a pedestrian during the summer daytime.

3. Results

3.1 Mesoscale calculation

Fine and sea breeze days extracted under the above conditions were 14, 11, and 6 days in Tokyo, Osaka, and Nagoya on August, and sea breeze days were 21, 15, and 11 days in Tokyo, Osaka, and Nagoya on August (Table 2). Most of the other days were affected by

typhoons and fronts. The calculated values and the observed values, which are hourly instantaneous values, are compared using the data from the observatory in domain 2 for each city. Figure 4 shows the locations of the measurement points. Since humidity is measured only at the points indicated by the large black circles, the measurement points of the air pollution monitoring stations, indicated by black squares, are added for comparison with the calculated values.

Table 2 Conditions and extraction results for fine and sea breeze days from August 1-31, 2010.

	Tokyo	Osaka	Nagoya	Conditions
Fine days	14	11	6	Weather: mostly sunny and sunny, Sunshine hours: more than 7.0 hours, Solar radiation: more than 19 MJ/m^2, Precipitation: less than 0.5 mm
Sea breeze days	21	15	11	Wind velocity: more than 2.0 m/s at observatory, Wind direction: main wind direction at each observatory, Duration time: more than 6 hours under the above conditions

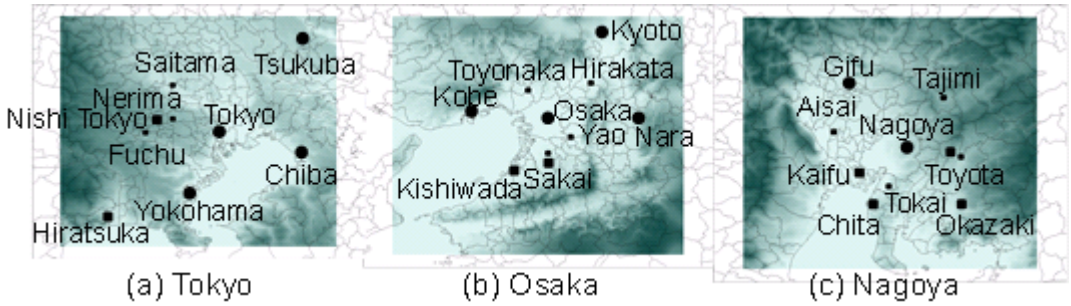

Figure 4 Locations of the measurement points in (a) Tokyo, (b) Osaka, and (c) Nagoya (103 km square).

Due to the limited number of measurement points, observation data from land use outside of urban areas are also used for verification. The bias, RMSE, and correlation between the calculated and observed values of air temperature, wind velocity, and humidity at each station in Tokyo, Osaka, and Nagoya are shown in Table 3. The accuracy of air temperature and wind velocity calculations is comparable to previous studies (Kitao et al., 2009 and Moriyama et al., 2014). The accuracy of the humidity calculation results is slightly worse at the air pollution monitoring stations indicated by the black squares in Figure 4. The number of measurement stations in Tokyo is 9, of which 4 are air pollution monitoring stations. The number of measurement stations in Osaka is 10, of which 2 are air pollution monitoring stations. The number of measurement stations in Nagoya is 10, of which 2 are air pollution monitoring stations. Most of the measurement stations are located in the metropolitan area of each city. The instruments of the air pollution monitoring stations are expected to have errors in accuracy. Since most of the measurement points in Tokyo, Osaka, and Nagoya are located in urban areas, local sources and sinks of water vapor near the measurement points are not assumed. However, it was determined that this would not have a significant impact on the study of the distribution of thermal environment indicators in urban areas.

Table 3 Bias, RMSE, and correlation between calculated and observed values of air temperature, wind velocity and humidity at each station in Tokyo, Osaka and Nagoya.

		Air temperature at 2m high	Humidity at 2m high	Wind velocity at 10m high

		Bias [°C]	RMSE [°C]	Correlation	Bias [g/kg]	RMSE [g/kg]	Correlation	Bias [m/s]	RMSE [m/s]	Correlation
Tokyo	Tokyo	0.50	0.72	0.92	0.15	0.53	0.51	-0.38	0.54	0.78
	Nerima	0.72	0.79	0.92				1.74	1.85	0.63
	Fuchu	1.80	2.14	0.90				0.01	0.72	0.70
	Saitama	1.13	1.19	0.91				0.41	0.72	0.69
	Tsukuba	0.82	0.88	0.94	0.38	0.48	0.60	0.73	0.95	0.74
	Chiba	-0.24	0.28	0.90	0.95	1.04	0.38	-0.97	1.03	0.78
	Yokohama	1.18	1.20	0.92	0.22	0.50	0.50	-0.17	0.23	0.79
	Nishi Tokyo	1.08	1.15	0.92	-3.85	3.86	0.54	0.47	0.55	0.74
	Hiratsuka	1.30	1.38	0.85	-1.25	1.27	0.52	1.04	1.26	0.42
Osaka	Osaka	0.20	0.31	0.92	0.74	0.77	0.70	-0.13	0.43	0.67
	Kobe	0.30	0.45	0.89	-0.95	1.01	0.71	-1.14	1.19	0.59
	Sakai	0.40	1.15	0.91				0.28	0.71	0.58
	Toyonaka	0.43	0.54	0.91				-0.18	0.52	0.62
	Yao	0.92	0.98	0.92				-0.71	0.92	0.56
	Hirakata	0.42	0.63	0.87				0.86	0.94	0.47
	Kyoto	0.33	0.37	0.90	0.95	0.97	0.72	-0.23	0.44	0.54
	Nara	1.61	1.73	0.89	-0.44	0.48	0.57	0.76	0.79	0.45
	Sakai	1.38	1.66	0.77	2.24	2.57	0.27	0.09	0.21	0.60
	Kishiwada	-0.39	1.02	0.87	3.67	3.74	0.32	0.52	0.69	0.55
Nagoya	Nagoya	0.71	0.80	0.90	0.84	0.95	0.66	-0.46	0.56	0.64
	Tokai	0.24	0.48	0.89				0.97	1.02	0.53
	Aisai	-0.18	0.32	0.93				1.37	1.52	0.62
	Toyota	0.59	0.75	0.93				0.42	0.58	0.33
	Gifu	0.97	1.01	0.90	0.89	0.95	0.72	-0.29	0.40	0.64
	Tajimi	0.47	0.84	0.93				0.46	0.59	0.53
	Toyota	-0.73	0.95	0.92	-0.88	1.02	0.64	0.71	0.80	0.40
	Okazaki	-0.04	0.57	0.93	-0.72	1.63	0.50	1.12	1.19	0.34
	Kaifu	-0.91	0.94	0.91	0.90	1.12	0.64	0.76	0.82	0.64
	Chita	0.11	0.68	0.85	-1.98	2.11	0.55	0.66	0.77	0.58

Figure 5 shows the distribution of air temperature, wind velocity, and humidity at 14:00 on a fine day (Tokyo: August 22, 2010; Osaka: August 21, 2010; Nagoya: August 26, 2010). In all three cities, coastal areas have cooler air temperatures, faster wind velocities, and higher humidity than inland areas. The intrusion of a sea breeze front can be clearly seen in the wind velocity distribution, especially in Tokyo and Osaka. In these two cities, the effects of the intrusion of the sea breeze front have also been observed in air temperature

distribution. In Tokyo, the humidity is higher in coastal areas and lower in inland areas, but this is not always clear in Osaka and Nagoya.

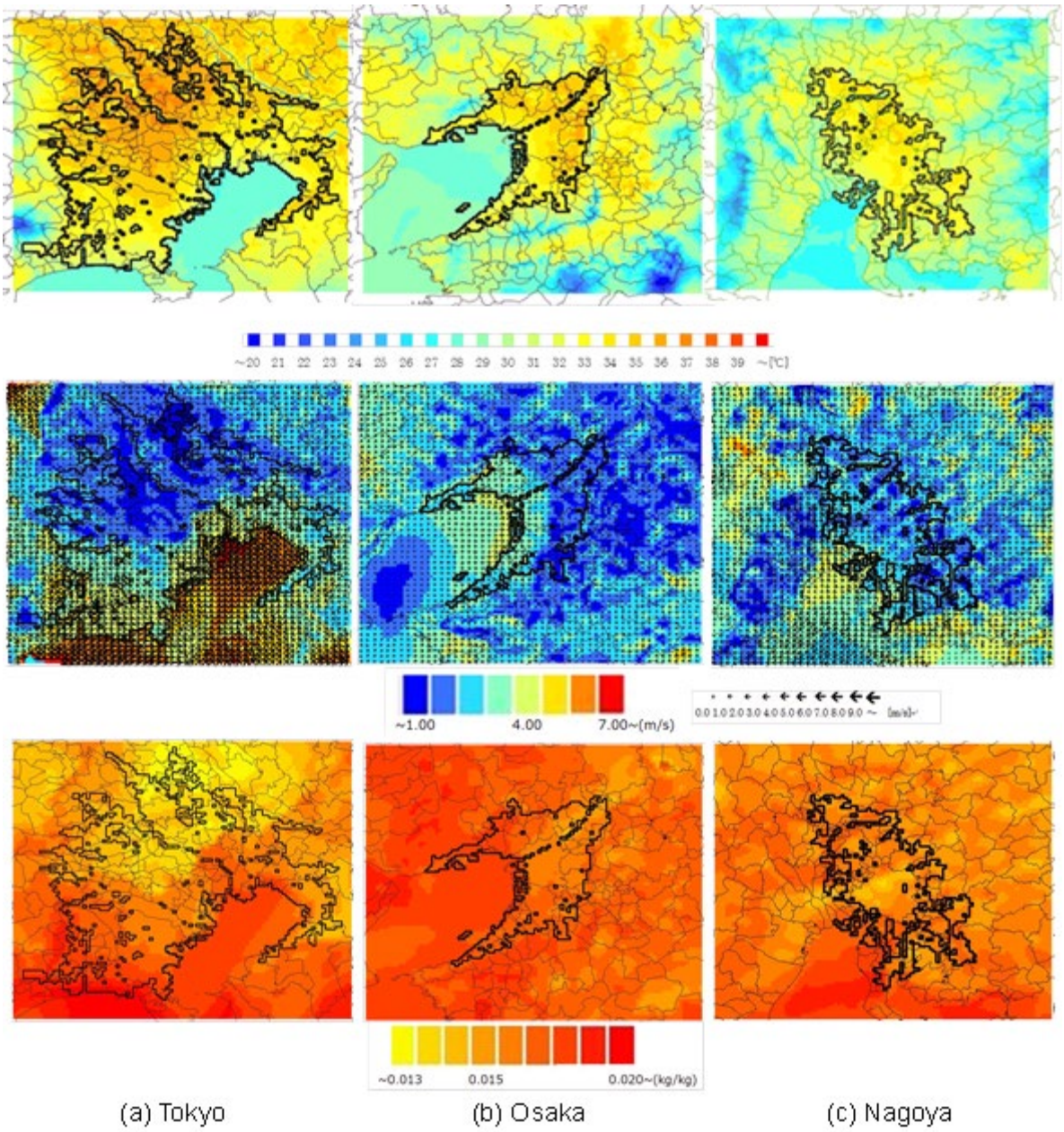

(a) Tokyo (b) Osaka (c) Nagoya

Figure 5 Distribution of air temperature, wind velocity, and humidity at 14:00 on a fine day in (a) Tokyo, (b) Osaka, and (c) Nagoya.

3.2 Indoor cooling load

Figure 6 shows the distribution of enthalpy, WBGT, SET*, and PET at 14:00 on a fine day in Tokyo, Osaka, and Nagoya. The outdoor specific enthalpy Ho is about 77 kJ/kg in coastal areas, which is about 1.5 kJ/kg (= ΔHo) greater than inland areas. The specific enthalpy Hi of the room shall be 53 kJ/kg at air temperature of 26°C and relative humidity of 50%. Therefore, the enthalpy increase rate ΔHo/(Ho-Hi) = 1.5/(77-53) = 6.3%. And since the ventilation cooling load Q is at most half of the total cooling load of the building, including the lighting load, equipment load, and heat transfer load from walls and windows, the effect of the high outdoor specific enthalpy ΔHo near the coast is only a few percent of the total indoor cooling load. The ventilation rate V varies depending on the ventilation needs of each building, but an increase in the dehumidification load has a smaller impact on primary energy consumption and CO2 emission.

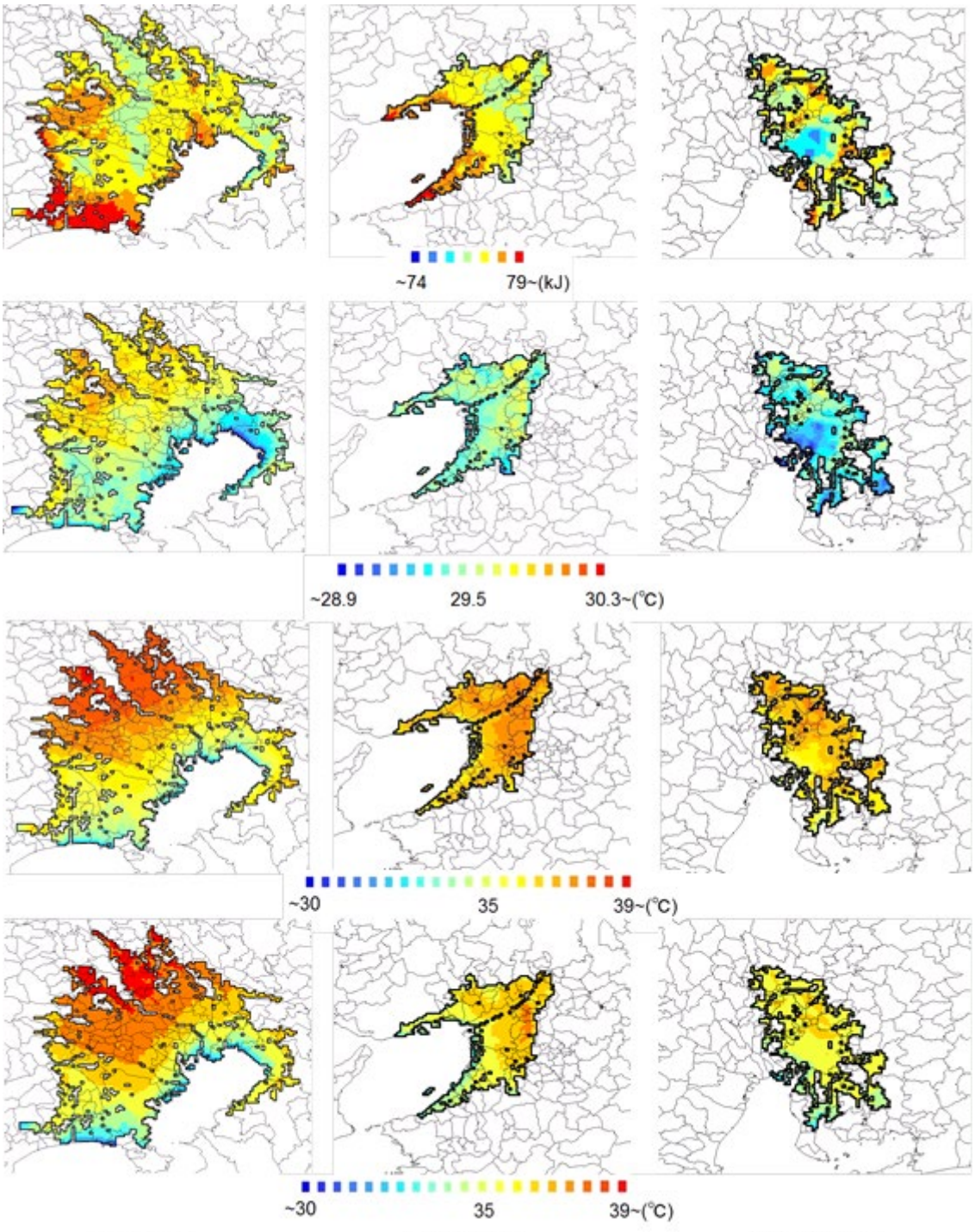

(a) Tokyo (b) Osaka (c) Nagoya

Figure 6 Distribution of enthalpy, WBGT, SET*, and PET at 14:00 on a fine day in (a)Tokyo, (b) Osaka, and (c)Nagoya.

3.3 Outdoor human thermal environment

In Figure 6, WBGT, SET*, and PET are higher in inland areas than in coastal areas, depending on the distribution of air temperature, humidity, and wind velocity at the urban scale, because the effects of local solar radiation shielding and urban ventilation are not considered. However, the difference in WBGT between coastal and inland areas is smaller than the difference in SET* and PET. This is because inland areas have lower humidity but higher air temperatures and lower wind velocities compared to coastal areas. The effect of wind velocity is not really reflected in the WBGT.

4. Discussion

The relationships between distance from the coast and SET*, air temperature, humidity and wind velocity on a fine sea breeze day are shown in Figure 7. It was at 14:00 on August 28th in Tokyo, 21st in Osaka, and 29th in Nagoya. A similar trend was observed on other fine sea breezy days, although it varied slightly from day to day in each city. Although the elevation and land use of each site are factors in the variation of each meteorological element, the relationships between SET*, air temperature and distance from the coast are confirmed. And the trend in SET* reflects that of air temperature in all cities. Humidity and wind velocity tend to be slightly higher near the coast, but there is no

clear relationship with the distance from the coast. The wind velocity varies greatly in and out of the sea breeze front as seen in Osaka, but since the sea breeze does not necessarily enter the inland area along the distance from the coast, it is difficult to recognize a clear change in wind velocity from the relationship diagrams as seen in Tokyo and Nagoya. It is considered that one of the reasons for the lack of a clear trend in humidity is that the path of the sea breeze is not necessarily in only one direction. In these areas, the wind direction of the sea breeze may change with time, and the time and distance of the sea breeze's entry also vary depending on the meteorological conditions, making it difficult to organize the spatial distribution of humidity and wind velocity by distance from the coast.

Table 4 shows air temperature, wind velocity, humidity, enthalpy, WBGT, SET*, PET and their differences between the coastal and inland areas at 14:00 mean on fine sea breeze days in the Tokyo, Osaka and Nagoya areas. The values near the coast and inland are extracted as the average values for each region from the distribution maps of the relationship between distance from the coast and each meteorological element, as shown in Figures 8-10, which are generated for each city. Coastal areas have cooler air temperatures, higher wind velocities, and higher humidity than inland areas. The difference between coastal and inland areas for these elements is larger in Tokyo than in Osaka and Nagoya. This is because urban land use (Urban A, B, and C) extends inland in Tokyo, as shown in Figure 3.

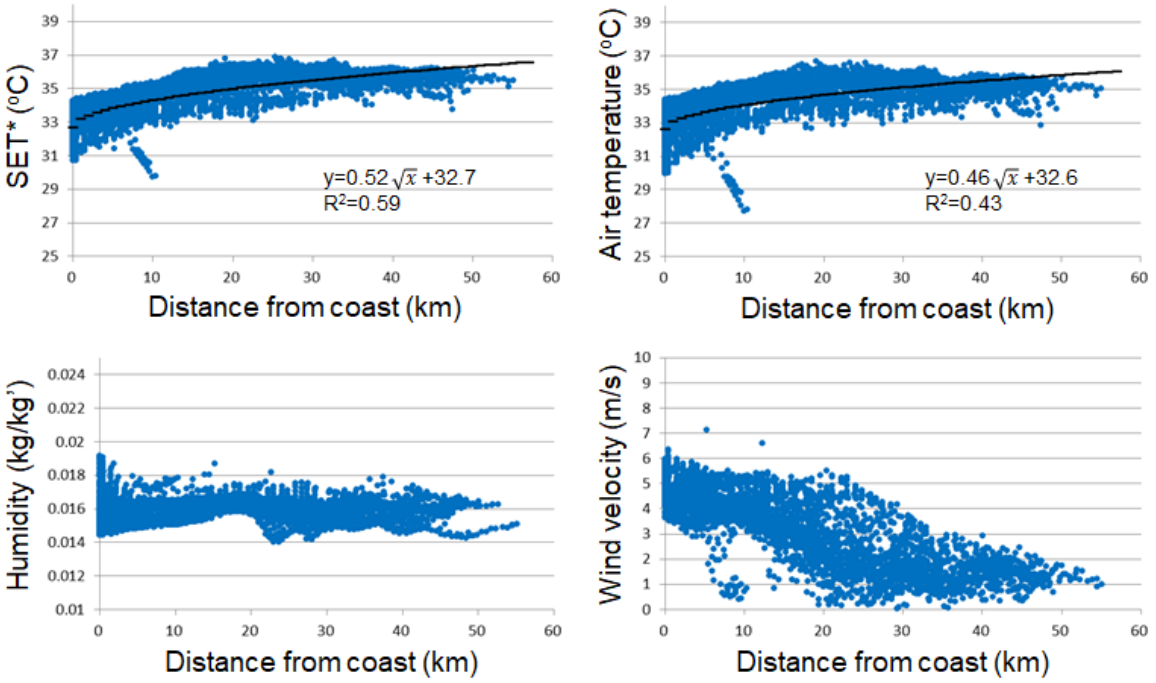

316

317 (a) at 14:00 on August 28th in Tokyo

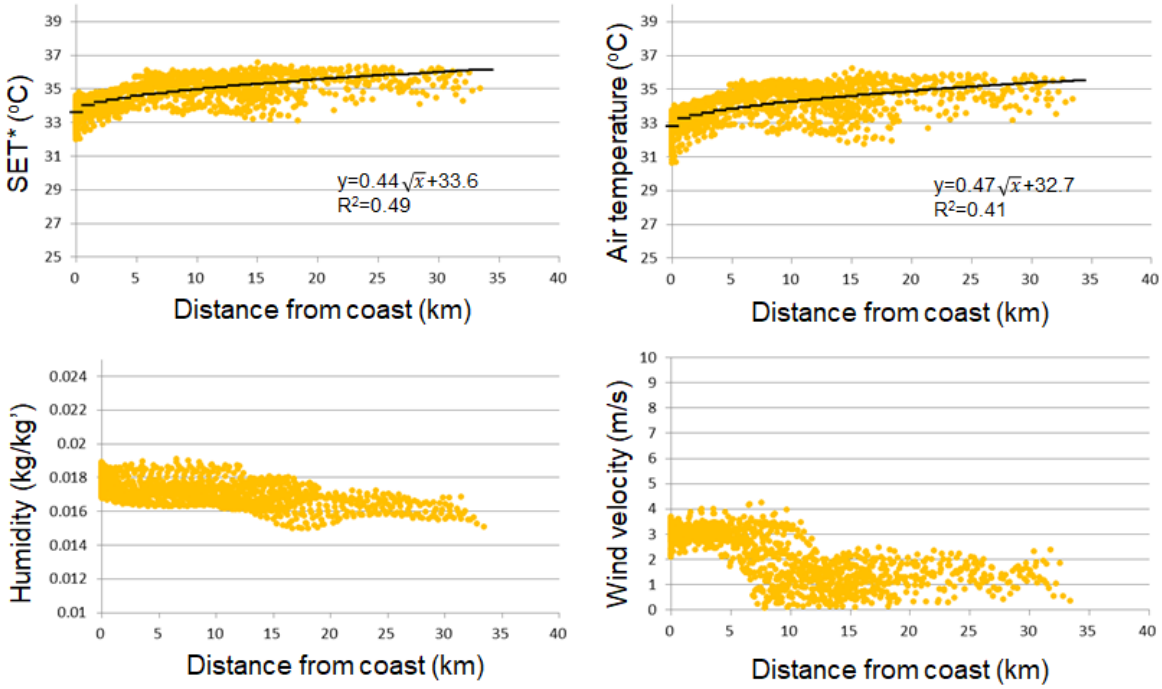

318

319 (b) at 14:00 on August 21st in Osaka

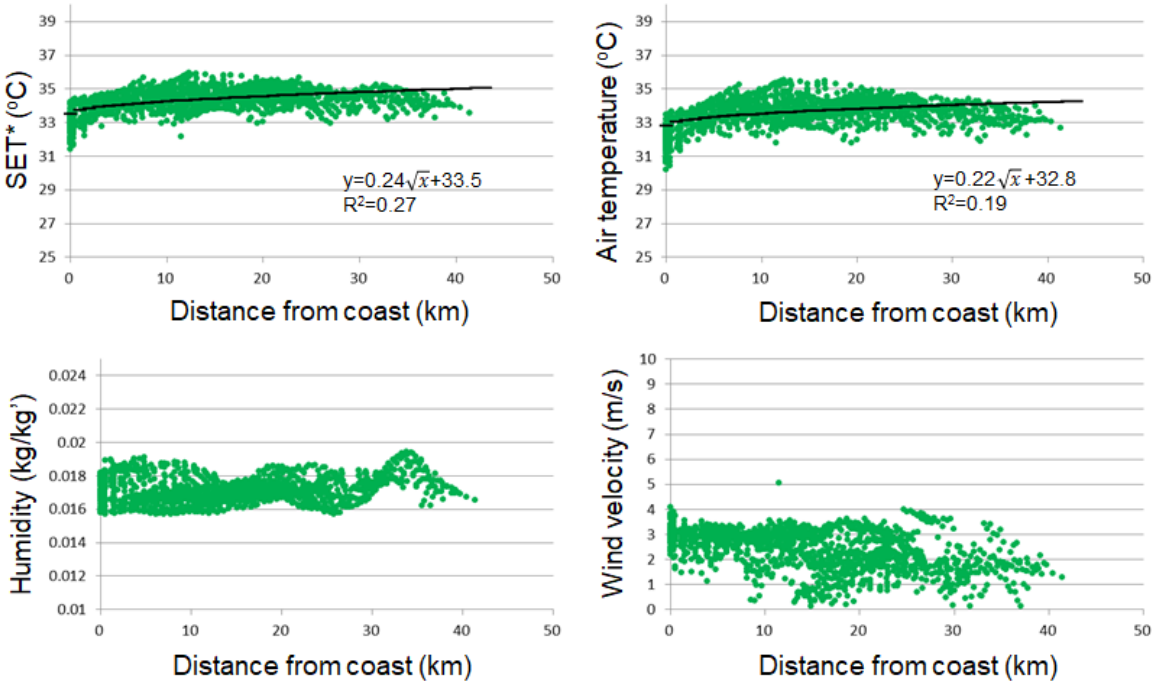

320

321 (c) at 14:00 on August 29th in Nagoya

322 Figure 7 Relationships between distance from the coast and SET*, air temperature,

323 humidity and wind velocity on a fine sea breeze day.

324

325 Table 4 Air temperature, wind velocity, humidity, enthalpy, WBGT, SET*, PET and their

326 differences between the coastal and inland areas at 14:00 mean on fine sea breeze days in

327 the Tokyo, Osaka and Nagoya areas.

	Air temperature (˚C) at 2m high			Wind velocity (m/s) at 10m high			Humidity (g/kg) at 2m high			Enthalpy (J) at 2m high		
	coastal	inland	difference	coastal	inland	difference	coastal	inland	difference	coastal	inland	difference
Tokyo	32.2	35.8	-3.6	5.1	2.3	2.8	17.6	16.0	1.6	77,413	77,148	265
Osaka	32.5	34.2	-1.7	3.0	1.9	1.1	17.9	16.6	1.3	78,423	76,949	1,474
Nagoya	32.0	33.5	-1.5	3.5	2.2	1.3	17.5	16.8	0.7	76,859	76,795	64
	WBGT (°C) at 2m high			SET* (°C) at 2m high			PET (°C) at 2m high					
	coastal	inland	difference	coastal	inland	difference	coastal	inland	difference			

Tokyo	31.0	31.4	-0.4	33.6	35.2	-1.6	35.4	38.4	-3.0
Osaka	31.2	31.1	0.1	33.9	34.4	-0.5	36.1	37.5	-1.4
Nagoya	30.9	31.1	-0.2	33.4	34.0	-0.6	35.6	37.1	-1.5

328

329 Figure 8 shows the approximate curves of distance from the coast and SET* rise at 14:00
330 on fine sea breeze days in Osaka. It is a curve that is proportional to the half power of the
331 distance in each day. Correspondingly, Figure 9 shows the approximate curves of distance
332 from the coast and air temperature rise at 14:00 on fine sea breeze days in Osaka.
333 Although urban A, B, and C are set as land use conditions, daytime air temperature
334 distribution dominated by the influence of sea breezes are explained by the distance from
335 the coast, not by land use. The increase in SET* roughly reflects the increase in air
336 temperature for each day. Table 5 shows weather conditions on fine sea breeze days in
337 Osaka. Since fine sea breeze days have already been extracted based on solar radiation,
338 sunshine hours, wind velocity, and wind direction, weather conditions do not vary
339 significantly within the objective days. The authors have confirmed in their previous
340 studies [19] that the trend of air temperature increase in inland areas is generally
341 consistent within each city, although it varies from day to day depending on the
342 meteorological field. Figure 10 shows the approximate curves of distance from the coast
343 and SET*, air temperature rise at 14:00 on fine sea breeze days averaged over Tokyo,
344 Osaka, Nagoya, respectively. As the authors discussed in their previous study [19], the
345 coefficient of the approximate curve of air temperature rise proportional to the half
346 power of the distance is about 0.5 in Tokyo and Osaka, while it is about 0.2 in Nagoya.
347 Correspondingly, the coefficient of the approximate curve of SET* rise proportional to the

348 half power of the distance is about 0.4-0.5 in Tokyo and Osaka, while it is about 0.2 in

349 Nagoya. These trends were almost the same on cloudy sea breezes days.

350

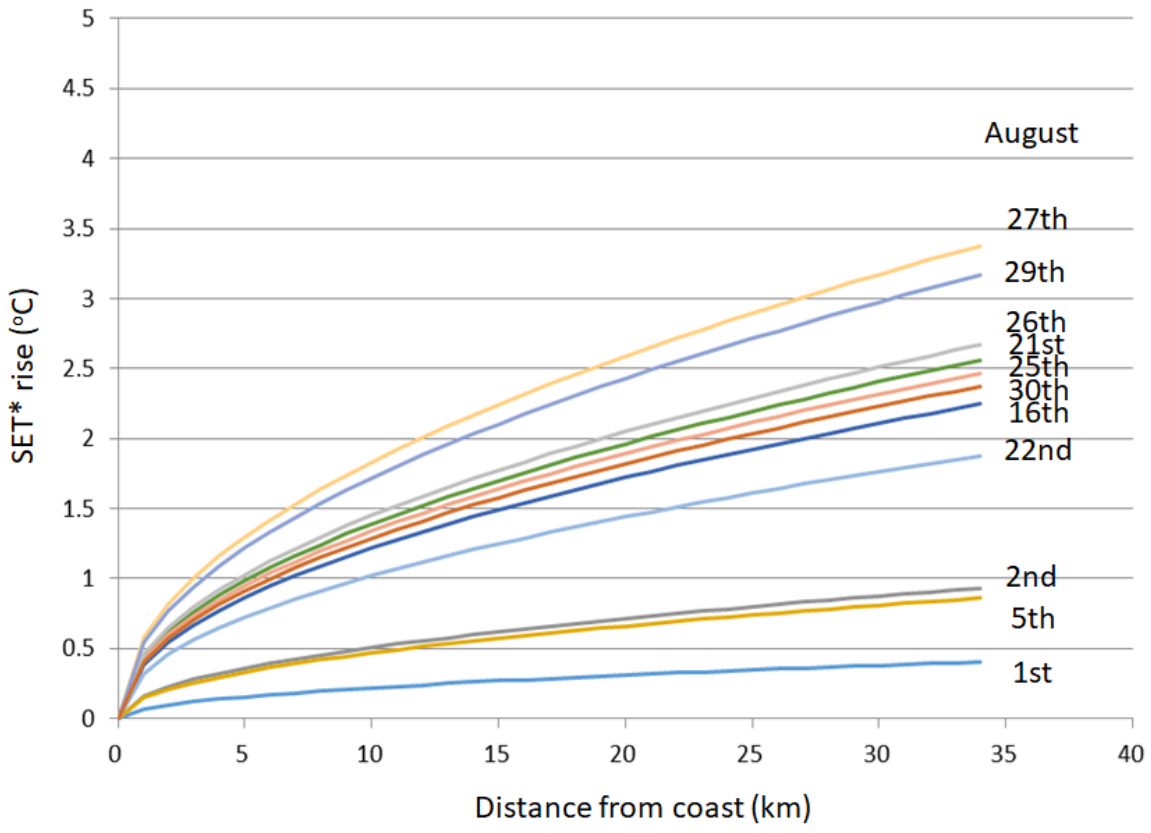

352 Figure 8 The approximate curves of distance from the coast and SET* rise at 14:00 on fine

353 sea breeze days in Osaka.

354

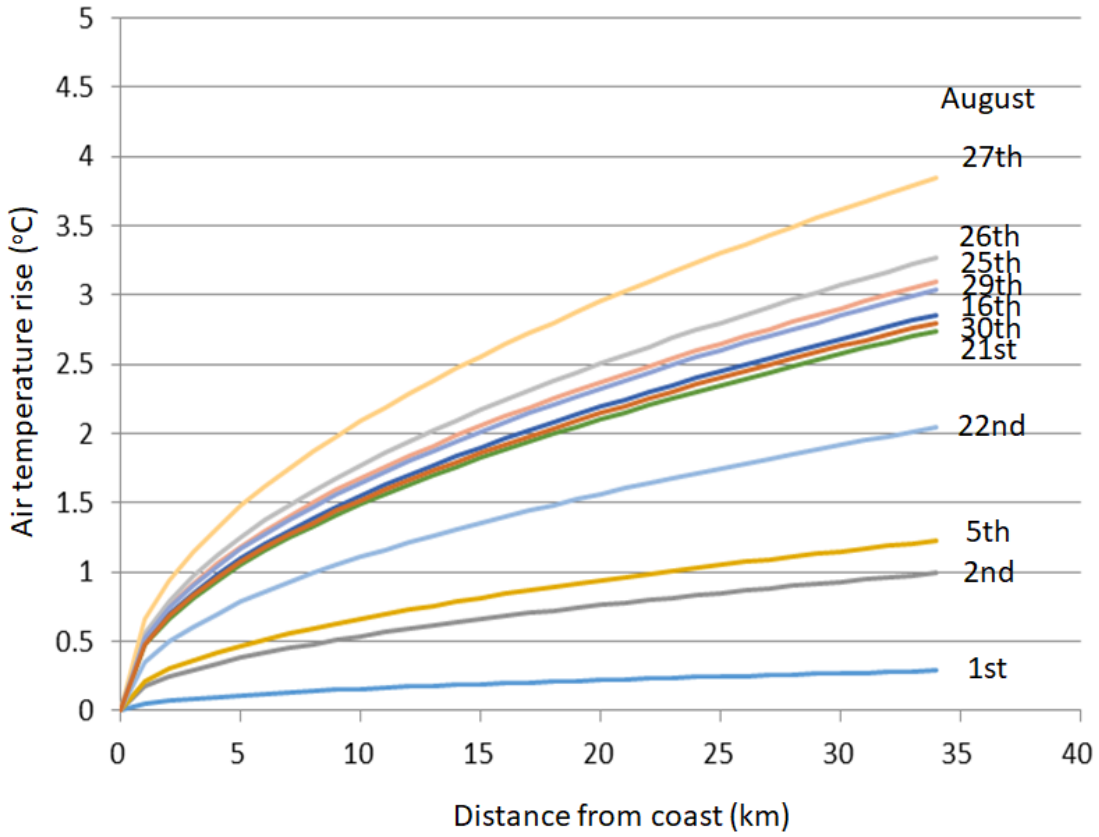

356 Figure 9 The approximate curves of distance from the coast and air temperature rise at

357 14:00 on fine sea breeze days in Osaka.

358

359 Table 5 Weather conditions on fine sea breeze days in Osaka.

Day	1	2	5	16	21	22	25	26	27	29	30
Daily integrated solar radiation (MJ/m^2)	23.5	19.9	21.9	23.4	22.0	22.1	20.4	21.7	22.1	23.7	20.1
Daily mean cloud cover (0-10)	6.0	5.3	3.5	5.5	6.3	5.8	3.8	2.8	7.8	6.8	5.5
Daily integrated sunshine hours (h)	9.1	8.2	9.9	10.5	8.1	8.8	8.5	11.1	8.5	10.8	9.1
Daily mean wind velocity (m/s)	2.9	2.0	2.6	2.9	2.8	2.4	3.2	2.5	2.4	2.7	2.5
Daily most frequent wind direction	W	W	W	WSW	W	W	WSW	W	W	W	W

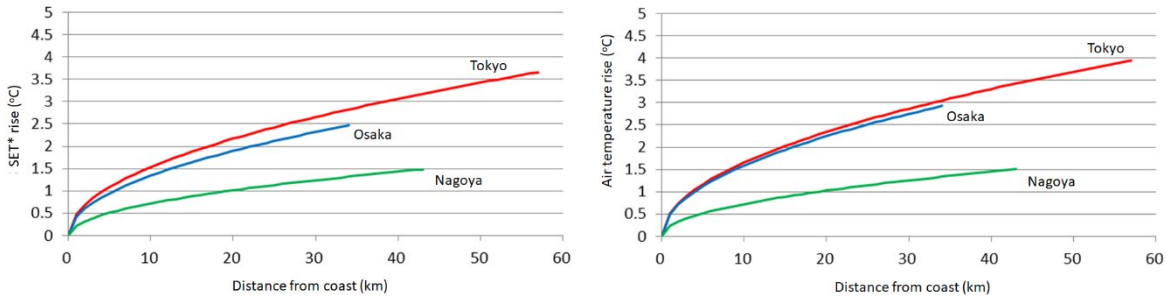

Figure 10 The approximate curves of distance from the coast and SET*, air temperature rise at 14:00 on fine sea breeze days averaged over Tokyo, Osaka, Nagoya, respectively.

The results of the above analysis show that as we move from inland to near the coast, air temperature decreases by about 1.5 to 3.6 °C, SET* decreases by about 1.4 to 3.4 °C, and WBGT decreases by about 0.1 to 0.6 °C. Moving from a sunny location to a shady location during a typical summer day can reduce SET* by about 5-8 °C and WBGT by about 1.5-2.5 °C, due to a large drop in mean radiant temperature, not air temperature [23]. When moving from a stagnant area to a well-ventilated area, SET* decreases by about 0-1.5 °C due to an increase in wind velocity below 1.0 m/s, not air temperature [23]. Ulpiani organized the decrease in air temperature and increase in relative humidity by reviewing research papers on water mist spraying [24]. She reported that air temperature could drop by 10-20 °C and the relative humidity could increase by a few to nearly 50 %, depending on the weather conditions. Under Japanese summer weather conditions, the decrease in air temperature is about 2 °C, which corresponds to an increase in relative

377 humidity of about 10% [5]. As a result, SET* decreases by about 2 °C and WBGT decreases
378 by about 0.1 °C. Table 6 shows a comparison of the effects of moving from inland to
379 coastal areas and introducing several types of adaptation measures. Solar shading is more
380 effective than moving to near the coast, urban ventilation, or mist spray. Rechecking
381 Figure 10 from a different perspective, the cooling effect of mist spraying in Tokyo and
382 Osaka corresponds to the effect of moving about 20 km from inland to near the coast. In
383 existing urban spaces, mist spraying and urban ventilation are also effective adaptation
384 measures. In addition to solar shading, mist spraying, and urban ventilation, watering,
385 evaporating pavement and walls, and greening pavement and walls are also envisioned as
386 adaptation measures. The effect of these measures can be calculated by replacing the
387 reduction in MRT and black-bulb temperature due to solar shading [6].
388
389 Table 6 Comparison of the effects of moving from inland to coastal areas and introducing
390 several types of adaptation measures.

	Moving to near the coast	Ventilation improvement	Mist spray	Solar shading
Air temperature (°C) reduction	1.5 - 3.6	-	2.0	-
SET* (°C) reduction	1.4 - 3.4	0 - 1.5	2.0	5 - 8
WBGT (°C) reduction	0.1 - 0.6	-	0.1	1.5 - 2.5

391

392 ## 5. Conclusion

393 The distribution of thermal environmental indices in the coastal cities of Tokyo, Osaka,
394 and Nagoya, where the increase in humidity due to the inflow of sea breezes may increase

the indoor cooling load and cause heat stoke, is analyzed to examine the possible adverse effects of increased humidity. In the three areas, the thermal environment indices WBGT, SET*, and PET are low due to low air temperatures and high wind velocities, although the humidity near the coast is high. The enthalpy increases slightly near the coast, but the effect on indoor cooling load is small. The daytime SET* distribution on sea breeze days is approximated by a curve proportional to the half power of the distance from the coast, similar to air temperature distribution. Changes in air temperature, humidity, and wind velocity associated with the inland penetration of sea breezes are examined, and the relationship between humidity, wind velocity and distance from the coast is not as clearly identified as the relationship between air temperature and distance from the coast. Because air temperature changes continuously in and out of the sea breeze front, while humidity and wind velocity vary greatly. As people move from inland to coastal areas, air temperature decreases by about 1.5-3.6 °C, SET* decreases by about 1.4-3.4 °C, and WBGT decreases by about 0.1-0.6 °C, respectively. As people move from inland to coastal areas, air temperature decreases by about 1.5-3.6 °C, SET* decreases by about 1.4-3.4 °C, WBGT decreases by about 0.1-0.6 °C. As people move from a sunny location to a shady location during a typical summer day, SET* decreases by about 5-8 °C and WBGT decreases by about 1.5-2.5 °C. Solar shading is more effective than moving to near the coast, urban ventilation and mist spray. However, although this paper has discussed at a resolution of 1 km, detailed discussions at smaller scales are also necessary.

Funding

This work was supported by JSPS KAKENHI grant number 16H04464.

References

[1] H. Akbari, D. Kolokotsa, Three decades of urban heat islands and mitigation technologies research. Energy and Buildings 2016, 133, 834-842, j.enbuild.2016.09.067.

[2] O. Aleksandrowicz, M. Vuckovic, K. Kiesel, A. Mahdavi, Current trends in urban heat island mitigation research: Observations based on a comprehensive research repository. Urban Climate 2017, 21, 1-26, j.uclim.2017.04.002.

[3] M. Santamouris, Cooling the cities – A review of reflective and green roof mitigation technologies to fight heat island and improve comfort in urban environments. Solar Energy 2014, 103, 682-703, j.solener.2012.07.003.

[4] M. Santamouris, Using cool pavements as a mitigation strategy to fight urban heat island—A review of the actual developments. Renewable and Sustainable Energy Reviews 2013, 26, 224-240, j.rser.2013.05.047.

[5] The Ministry of the Environment of Japan, Heat countermeasure guideline in the city. Available online: http://www.env.go.jp/air/life/heat_island/guidelineH30/gudelineH30_all.pdf (accessed on 10 December 2018).

436 [6] H. Takebayashi, A Simple Method to Evaluate Adaptation Measures for Urban Heat
437 Island. Environments 2018, 5, 70, 1-13, 10.3390/environments5060070.
438 [7] H. Takebayashi, Y. Kiyama, N. Yamamoto, Analysis of wind and radiant environment in
439 street canyons for production of urban climate maps at district scale, Journal of Heat
440 Island Institute International 2017, 12(2), 78-83.
441 [8] Y. Ohashi, Y. Kikegawa, T. Ihara, N. Sugiyama, Numerical simulations of outdoor heat
442 stress index and heat disorder risk in the 23 wards of Tokyo, Journal of Applied
443 Meteorology and Climatology 2014, 53, 583-597, 10.1175/JAMC-D-13-0127.1.
444 [9] Y. Ohashi, T. Ihara, Y. Kikegawa, N. Sugiyama, Numerical simulations of influence of
445 heat island countermeasures on outdoor human stress in the 23 wards of Tokyo,
446 Japan, Energy and Buildings 2016, 144, 104-111, 10.1016/j.enbuild.2015.06.027.
447 [10] M. Kasai, T. Okaze, M. Yamamoto, A. Mochida, K. Hanaoka, Summer heatstroke risk
448 prediction for Tokyo in the 2030s based on mesoscale simulations by WRF, Journal of
449 Heat Island Institute International 2017, 12(2), 61-67.
450 [11] I. Eliasson, Urban Geometry, surface temperature and air temperature. Energy and
451 Buildings 1990, 15, 141–145, 10.1016/0378-7788(90)90125-3.
452 [12] F. Ali-Toudert, H. Mayer, Numerical study on the effects of aspect ratio and
453 orientation of an urban street canyon on outdoor thermal comfort in hot and dry
454 climate. Building and Environment 2006, 41, 94–108, 10.1016/j.buildenv.2005.01.013.

[13] F. Ali-Toudert, H. Mayer, Effects of asymmetry, galleries, overhanging façades and vegetation on thermal comfort in urban street canyons. Solar Energy 2007, 81, 742–754, 10.1016/j.solener.2006.10.007.

[14] L. Martinelli, T.P. Lin, A. Matzarakis, Assessment of the influence of daily shadings pattern on human thermal comfort and attendance in Rome during summer period. Building and Environment 2015, 92, 30–38, 10.1016/j.buildenv.2015.04.013.

[15] L.V. Abreu-Harbich, L.C. Labaki, A. Matzarakis, Effect of tree planting design and tree species on human thermal comfort in the tropics. Landscape and Urban Planning 2015, 138, 99–109, 10.1016/j.landurbplan.2015.02.008.

[16] J.A.R. Algeciras, L.G. Consuegra, A. Matzarakis, Spatial-temporal study on the effects of urban street configurations on human thermal comfort in the world heritage city of Camagüey-Cuba. Building and Environment 2016, 101, 85–101, 10.1016/j.buildenv.2016.02.026.

[17] H. Lee, H. Mayer, L. Chen, Contribution of trees and grasslands to the mitigation of human heat stress in a residential district of Freiburg, Southwest Germany. Landscape and Urban Planning 2016, 148, 37–50, 10.1016/j.landurbplan.2015.12.004.

[18] S. Zheng, L. Zhao, Q. Li, Numerical simulation of the impact of different vegetation species on the outdoor thermal environment. Urban Forestry & Urban Greening 2016, 18, 138–150, 10.1016/j.ufug.2016.05.008.

[19] H. Takebayashi, T. Tanaka, M. Moriyama, H. Watanabe, M. Miyazaki, K. Kittaka, Relationship between city size, coastal land use, and summer daytime air temperature rise with distance from coast, climate 2018, 6, 84, 1-13, 10.3390/cli6040084.

[20] National Center for Atmospheric Research, Weather Research & Forecasting Model. Available online: https://www.mmm.ucar.edu/weather-research-and-forecasting-model (accessed on 24 May 2020).

[21] H. Kusaka, H. Kondo, Y. Kikegawa, F. Kimura, A simple single-layer urban canopy model for atmospheric models, Comparison with multi-layer and slab models. Boundary Layer Meteorology 2001, 101, 261–304. 10.1023/A:1019207923078.

[22] N. Kitao, M. Moriyama, S. Nakajima, T. Tanaka, H. Takebayashi, The characteristics of urban heat island based on the comparison of temperature and wind field between present land cover and potential natural land cover. In Proceedings of the Seventh International Conference on Urban Climate, Yokohama, Japan, 29 June–3 July 2009.

[23] H. Takebayashi, Thermal environmental design of outdoor spaces by examining redevelopment building opposite central Osaka station. Climate 2019, 7, 143, 1-11, 10.3390/cli7120143.

[24] G. Ulpiani, Water mist spray for outdoor cooling: A systematic review of technologies, methods and impacts, Applied Energy 2019, 254, 1136-1147, 10.1016/j.apenergy.2019.113647.